

RESEARCH ARTICLE | JULY 25 2024

Beyond the blur: Using experimentally determined point spread functions to improve scanning Kelvin probe imaging

Isaac C. D. Lenton ; Felix Pertl ; Lubuna Shafeek ; Scott R. Waitukaitis

Check for updates

J. Appl. Phys. 136, 045305 (2024)

<https://doi.org/10.1063/5.0215151>



05 August 2024 08:19:08

Nanotechnology & Materials Science


Optics & Photonics

Impedance Analysis

Scanning Probe Microscopy


Sensors

Failure Analysis & Semiconductors



Unlock the Full Spectrum.
From DC to 8.5 GHz.
Your Application. Measured.

[Find out more](#)



Beyond the blur: Using experimentally determined point spread functions to improve scanning Kelvin probe imaging

Cite as: J. Appl. Phys. 136, 045305 (2024); doi: 10.1063/5.0215151

Submitted: 22 April 2024 · Accepted: 9 July 2024 ·

Published Online: 25 July 2024



Isaac C. D. Lenton,^{a)} Felix Pertl, Lubuna Shafeek, and Scott R. Waitukaitis

AFFILIATIONS

Institute of Science and Technology Austria, Am Campus 1, 3400 Klosterneuburg, Austria

^{a)}Author to whom correspondence should be addressed: isaac.lenton@ist.ac.at

ABSTRACT

Scanning Kelvin probe microscopy (SKPM) is a powerful technique for investigating the electrostatic properties of material surfaces, enabling the imaging of variations in work function, topology, surface charge density, or combinations thereof. Regardless of the underlying signal source, SKPM results in a voltage image, which is spatially distorted due to the finite size of the probe, long-range electrostatic interactions, mechanical and electrical noise, and the finite response time of the electronics. In order to recover the underlying signal, it is necessary to deconvolve the measurement with an appropriate point spread function (PSF) that accounts the aforementioned distortions, but determining this PSF is difficult. Here, we describe how such PSFs can be determined experimentally and show how they can be used to recover the underlying information of interest. We first consider the physical principles that enable SKPM and discuss how these affect the system PSF. We then show how one can experimentally measure PSFs by looking at well-defined features, and that these compare well to simulated PSFs, provided scans are performed extremely slowly and carefully. Next, we work at realistic scan speeds and show that the idealized PSFs fail to capture temporal distortions in the scan direction. While simulating PSFs for these situations would be quite challenging, we show that measuring PSFs with similar scan conditions works well. Our approach clarifies the basic principles and inherent challenges to SKPM measurements and gives practical methods to improve results.

© 2024 Author(s). All article content, except where otherwise noted, is licensed under a Creative Commons Attribution-NonCommercial-NoDerivs 4.0 International (CC BY-NC-ND) license (<https://creativecommons.org/licenses/by-nc-nd/4.0/>). <https://doi.org/10.1063/5.0215151>

I. INTRODUCTION

Scanning Kelvin probe microscopy (SKPM) enables imaging of the “invisible” electrostatic properties of surfaces at the mesoscale (typically, $> 100 \mu\text{m}$). By scanning a vibrating conductive probe above a surface and measuring/regulating the current induced within it [Fig. 1(a)], SKPM extracts information connected to the local electric potential.^{1,2} This gives insight into various processes such as variations in work function or surface chemistry,^{3,4} charge,^{5,6} biological double layers,^{7,8} etc. Though not identical, the operating principle behind SKPM is related to Kelvin probe force microscopy (KPFM),⁹ where measurement/regulation of the forces acting on a vibrating atomic force microscope tip permits similar imaging at the nanoscale.^{10–12} One major advantage of SKPM over KPFM is the use of significantly larger probes enabling rapid scans over significantly larger areas (a discussion on the differences/similarities between the two techniques is included in the [supplementary material](#)).

A fundamental problem in both SKPM and KPFM is properly interpreting and analyzing the measured signal. Regardless of the signal source (e.g., work function variations or charge), both techniques produce voltage images. Moreover, these images are spatially distorted due to the finite size of the probe, long-range electrostatic interactions,^{13,14} mechanical and electrical noise,¹⁵ and the temporal response of the electronics.^{2,16,17} When these distortions are deterministic and linear, they can be characterized by a point spread function (PSF), which describes the image as an infinitesimally small point in the absence of noise would produce when measured. Effectively, the measured signal is the convolution of the underlying signal with the PSF, and the underlying signal can be recovered by deconvolution.^{13,14} Therefore, a key component in interpreting/analyzing SKPM (or KPFM) data relies on being able to determine the PSF that characterizes the measurement process.

05 August 2024 08:19:08

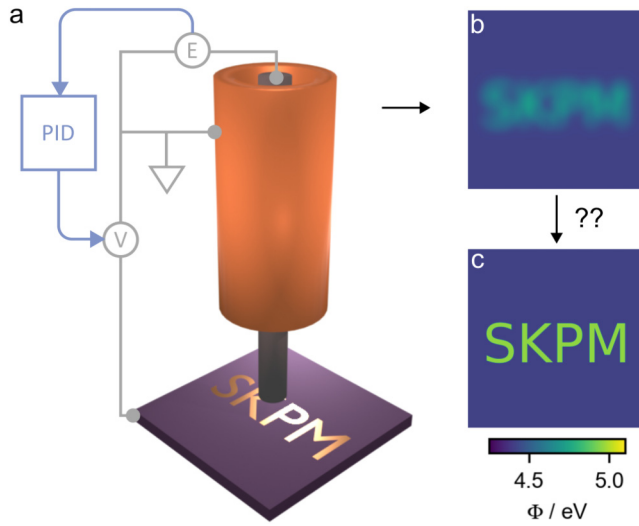


FIG. 1. Principle of scanning Kelvin probe microscopy (SKPM). (a) SKPM entails scanning a conductive probe above a sample to estimate the local surface potential. The cylindrical metal probe is vibrated vertically, while a lock-in amplifier and PID use feedback to adjust the backing potential, V , so that the current in the probe is minimized. (b) Voltage maps measured by SKPM are spatially distorted, due to the probe's finite size, long-range electrostatics, and the temporal response of the electronics. (c) This paper is about extracting the true underlying surface potential from the measured signal, which we show is achievable by experimentally measuring the system's PSF and using this to deconvolve raw measurements.

Toward addressing the problem, one can draw inspiration from optical microscopy. Like SKPM, optical images suffer from distortions due to diffraction, optical imperfections, finite pixel sizes, etc. To correct for these, a practical solution is to image the pattern created by a point-like emitter, e.g., a small fluorescent particle.¹⁸ When this target is significantly smaller than the system resolution, the image rendered is approximately the PSF.

Here, we show that the approach of experimentally measuring PSFs is not only viable but also effective and straightforwardly implemented in the case of SKPM. Compared to KPFM, the larger probes used in SKPM allow scanning significantly larger areas at higher scan rates. Consequently, for SKPM it is possible to experimentally measure the PSFs using relatively large calibration targets. We restrict ourselves to situation where the underlying signal is due to differences in material work functions on a planar surface, though in principle our ideas can be extended to other situations (e.g., variations in surface charge). We use common clean-room techniques to pattern regions with work function differences, which we image to extract PSFs. We find that when utilizing high scan speeds—which are necessary to probe large and/or time dependent features—the measured PSFs can differ significantly from those that only account for the electrostatic interactions between the probe and sample. We show that this is due to the incorporation of temporal information into the PSF—an issue that would be difficult to account for analytically/computationally, but that is solved relatively easily in the experiment. By simply measuring

the PSF, we gain insight into the effect of measurement speed, feedback parameters, and probe geometry that would be difficult to predict or characterize independently. Our results outline a practical and easily implemented approach toward getting quantitative information out of SKPM.

II. MEASUREMENT PRINCIPAL

A. Signal acquisition

Figure 1(a) depicts an SKPM probe positioned above a sample and the feedback system used to acquire an estimate for the spatially varying surface potential of interest, $V_S \equiv V_S(x)$. The probe vibrates vertically at a fixed amplitude and frequency, while a potential (V) is applied to the electrode at or below the sample. The current drawn to the probe due to the vibration is measured by an electrometer (E) and further amplified by a lock-in amplifier, which extracts the current signal due to the probe vibration and rejects noise at other frequencies. The signal acquired by SKPM is the value of the voltage, V , required to minimize the current induced in the probe as it is vibrated. This is typically accomplished by using feedback on the lock-in signal, e.g., sending it to proportional-integral-differential (PID) electronics and adjusting V until the current amplitude is zero. In the naïve version of the analysis, the probe-sample system is assumed to form a capacitor, where the image charge drawn to the probe is given by

$$Q(t) = C(h(t))(V - V_S). \quad (1)$$

Here, $C(h)$ is the capacitance and $h(t)$ is the time-varying height of the probe above the sample. By differentiating Eq. (1) with respect to time, setting equal to zero, and defining for $V_m \equiv V$ in this condition, we find

$$0 = \frac{dQ}{dt} = \frac{dh}{dt} \frac{dC}{dh} (V_m - V_S). \quad (2)$$

Hence, for finite derivatives dh/dt and dC/dh , we see that this condition is satisfied when

$$V_m(x) = V_S(x). \quad (3)$$

In other words, the simplest interpretation of raw SKPM data is that it is an exact, point-by-point copy of the surface potential of interest.

The above analysis does not account for the finite size of the probe or long-range electrostatic interactions. These contributions can be incorporated by replacing the simple capacitance, $C(h)$, with an integral over a distributed capacitance, $\mathcal{C}(h, x)$.^{13,14} In this case, the SKPM condition becomes

$$0 = \frac{d}{dh} \int_S (V_m(x) - V_S(\xi - x)) \mathcal{C}(h, \xi) d\xi, \quad (4)$$

where ξ is an integration variable. Solving this expression for V_m

05 August 2024 08:19:08

gives

$$V_m(x) = \int_S P(x, \xi) V_S(\xi) d\xi, \quad (5)$$

where we define the PSF, $P(x, \xi)$, which accounts for the terms involving the interaction of the probe at location x with different sample positions ξ . Hence, a slightly more sophisticated analysis reveals that a raw SKPM measurement is the convolution of the underlying signal with a point spread function corresponding to the finite size of the probe and long-range interactions. It is important to note that the PSF is not unique for a particular probe. Instead, it depends on the sample-probe interaction through the distributed capacitance. For example, this may give rise to completely different PSFs for purely metallic, purely insulating, or mixed insulator-metal samples due to how the probe interacts with the surface or the bulk of the material.¹⁹

In practice, the situation is more complicated still, though for less obvious reasons. The measured signal depends not only on the electrostatic interactions between the probe and the sample but also on the feedback system that measures the current and applies the voltage, V . Both the PID and lock-in amplifier require finite response times to produce stable signals. If the probe travels a significant distance over these timescales, then information from a range of locations is incorporated into the measurement. Additionally, faster scan speeds can introduce additional mechanical noise, which will further distort the measured signal. Only for a stable system and when the probe is held at each location for a long time relative to the response times of the PID/lock-in, do we recover Eq. (5). Assuming these processes are linear, we can still write the measured voltage as a purely spatial convolution over a point spread function, but one that is velocity dependent; in other words,

$$V_m(x) = \int P(v|x, \xi) V_S(\xi) d\xi. \quad (6)$$

As the scan velocity approaches zero, $P(v|x, \xi) \rightarrow P(x, \xi)$, and the “fast scan” regime [Eq. (6)] becomes equivalent to the “slow scan” regime [Eq. (5)].

B. Signal deconvolution

In Sec. II A, we discussed the forward problem: given an underlying surface potential, $V_S(x)$, determine the resulting measurement, $V_m(x)$. However, what is usually required is the solution to the inverse problem: given the measurement, $V_m(x)$, determine the underlying signal, $V_S(x)$ [i.e., recover Fig. 1(c) from Fig. 1(b)]. We start by writing the convolution over the PSF more compactly as

$$V_m = V_S \otimes P. \quad (7)$$

We would like to find an estimate for the true surface voltage map, \bar{V}_S . In the absence of measurement noise, and for a non-vanishing P , we can exactly recover the true surface voltage map, V_S , by

$$\bar{V}_S = V_m \otimes P^{-1} = (V_S \otimes P) \otimes P^{-1} = V_S, \quad (8)$$

where $\otimes P^{-1}$ denotes the deconvolution with respect to P . This expression is relatively easy to calculate by taking advantage of the convolution theorem, i.e.,

$$\bar{V}_S = \mathcal{F}^{-1} \left(\frac{\mathcal{F}(V_m)}{\mathcal{F}(P)} \right), \quad (9)$$

where \mathcal{F} and \mathcal{F}^{-1} represent the Fourier transform and inverse Fourier transform, respectively.

Real systems suffer from measurement noise, which renders the equivalence of \bar{V}_S and V_S in Eq. (8) unattainable in practice. Mathematically, independent sources of noise, N , enter into the equation as $V_m = V_S \otimes P + N$ and contain high-frequency components, which deconvolution can amplify. To reduce the effect of this, one approach is to simply apply a low-pass filter to V_m , which can be heuristically motivated given the finite size of probes.²⁰ However, in order to avoid discarding higher frequency information unnecessarily, an alternative is to use a weighted deconvolution, such as a Wiener filter.^{13,14} Mathematically, this manifests itself as a modification to Eq. (9),

$$\bar{V}_S = \mathcal{F}^{-1} \left(\frac{\mathcal{F}(V_m)}{\mathcal{F}(P)} \times \left(\frac{|\mathcal{F}(P)|^2}{|\mathcal{F}(P)|^2 + \frac{1}{\text{SNR}(f)}} \right) \right), \quad (10)$$

where $\text{SNR}(f)$ is the signal-to-noise ratio as a function of spatial frequency. The SNR can either be measured (e.g., by calculating the power spectral density of representative samples with known properties) or, in certain circumstances, assumed in conjunction with a frequency-relationship for the noise (e.g., Brownian noise $1/f^2$ and pink noise $1/f$).

III. TARGET FABRICATION & MEASUREMENT

To experimentally determine the PSFs, we fabricate calibration targets using materials with different work functions. We work with two different types: an edge target, which produces a large signal but only provides information about the PSF in one direction,^{21,22} and a disk target, which allows convenient measurement of the full two-dimensional PSF from a single two-dimensional scan. We utilize the edge target for measuring the slow scan PSF [Eq. (5)], where we assume rotational symmetry of the PSF and are interested in a very accurate low noise estimate for the probe PSF. We use the disk target for estimating the fast scan PSF [Eq. (6)], where the PSF is highly non-axisymmetric and our priority is on performing measurements in reasonable amounts of time under practical conditions.

We fabricate both targets using electron beam evaporation to deposit thin layers of different metals; full details are provided in the [supplemental material](#). The edge target consists of a layer of platinum deposited on a titanium coated glass slide. The physical height of the platinum layer is small (12 nm) compared to the sample-tip separation (60 μm) so that its geometric influence can be ignored. These metals are chosen for their relatively large work function difference, which due to Fermi equalization leads to a large contact potential difference and correspondingly large SKPM signal (~ 1 V). The disk target consists of a small, circular

(400 μm diameter) gold disk deposited on a silicon wafer, creating a contact potential difference on the order of 0.5 eV. As with the edge target, the height of the gold–titanium disk is small (103 nm) compared to the scan height. Optical microscopy images of the disk calibration targets are included in the [supplementary material](#).

We perform SKPM measurements using a commercially available device (Biologic, M470). This instrument uses a piezo to oscillate the probe, we use an oscillation frequency of 80 Hz as we notice higher frequencies increase acoustic noise. The oscillation frequency sets limit on the measurement bandwidth and the achievable resolution at higher scan speeds, as we discuss further in Sec. IV B. We use a closed-loop type SKPM measurement, where a PID feedback controller attempts to minimize the current in the probe. The choice of feedback parameters is important to achieving the best possible bandwidth: too slow a response rate will lead to a broader PSF, while overly aggressive settings can lead to spurious oscillations in the measured signal. Briefly, we use the Ziegler–Nichols method²³ to choose initial guesses for the feedback settings and then make minor adjustments to optimize the results (further details provided in the [supplementary material](#)).

When SKPM is used for work function measurements, the signal ($\Delta\Phi$) is a relative measurement of the difference in work function between the probe and sample. To convert Kelvin probe voltages to absolute work function values, we use a reference sample of highly ordered pyrolytic graphite (HOPG),^{24,25} additional details are given in the [supplementary material](#). The work function is then given by $\Phi = \Delta\Phi + \Delta\Phi_{\text{HOPG}}$, where $\Delta\Phi_{\text{HOPG}}$ is the difference between the literature value for the HOPG work function and the measured value. To estimate the SNR for deconvolution [i.e., Eq. (10)], we look at the power spectral density of a relatively flat region and use this to estimate a power-law relationship between SNR and frequency.

To demonstrate the effect of acquisition parameters and the temporal dependence of acquired measurements, we perform slow scans with step-mode acquisition and fast scans with sweep-mode acquisition. The step-mode acquisition entails moving the probe between specific points and holding it fixed until the SKPM signal has stabilized (i.e., until we can ignore effects from the movement and settling time of the PID/lock-in amplifier). Sweep-mode acquisition involves moving the probe continuously across the sample at a constant velocity, resulting in a temporally distorted signal depending on the scan speed and feedback parameters.

IV. RESULTS AND DISCUSSION

A. Experimentally determining PSFs in the quasi-static limit

We now demonstrate how a PSF can be determined experimentally. We start in the slow scan regime, i.e., at speeds that are small enough such that Eq. (5) applies. The main difficulty in measuring the slow scan PSF is signal strength compared to measurement noise. Signal strength can be improved by increasing the work function difference between the target and surface or increasing the size of the target, while noise can be reduced with repeated measurements and reduced scan speed. We have found that a good solution for the slow-scan regime is to perform a one-dimensional scan over a sharp edge between two materials with distinct work

functions [Fig. 2(a)]. Sharp edges are a common technique for estimating the accuracy and resolution of both SKPM and KPFM systems^{26–28} and can provide enough information to estimate the PSF for a large cylindrical probe. Even so, extremely slow speeds are required for probe motion to be completely negligible. We utilize a step size of 5 μm , moving at 5 $\mu\text{m}/\text{s}$ between points and dwelling at each point for 3.5 s. To improve SNR, we repeat and average multiple lines. In this process, a *single* line scan takes approximately 45 min, and the ensemble takes more than 7 h. The final result is shown in Fig. 2(b).

To obtain the PSF, we first average multiple scans of the edge to produce a low noise estimate for the edge spread function (ESF). We then calculate the line spread function (LSF) from the derivative of the line scan

$$\text{LSF}(x) = \frac{d}{dx} \text{ESF}(x). \quad (11)$$

In Fourier space, we interpolate the one-dimensional transform of the line spread function to a two-dimensional map assuming rotational symmetry and take the inverse Fourier transform to give the PSF. Equivalently, we solve

$$\mathcal{F}_{2D}[\text{PSF}](k_i, k_j) = \mathcal{F}_{1D}[\text{LSF}]\left(\sqrt{k_i^2 + k_j^2}\right)$$

for the PSF, where \mathcal{F}_{1D} and \mathcal{F}_{2D} denote the 1D and 2D Fourier transforms, and k_i, k_j are the Fourier space coordinates (see the [supplementary material](#) for full details). The result is shown in [Fig. 2(c)]. The cross section of this PSF [Fig. 2(e)] has a non-intuitive feature: a ring of higher intensity toward the edge of the probe. To investigate this further and perform a sanity-check of our strategy, we perform numerical simulations for a second, independent estimate of the PSF [Figs. 2(d) and 2(e); see the [supplementary material](#) for details on simulations]. In addition, the PSF also has an apparent negative region at around $\pm 0.8 \text{ mm}$; however, this measurement is not statistically significant.

The simulations produce a decent estimate for the PSF, but the differences are non-negligible. The simulated PSF has a higher amplitude, is slightly narrower, and exhibits a more subdued ring at the edge. We suspect these differences are due to physical features of the probe that the idealized simulation geometry cannot capture. Our first thought was that the difference was related to an incomplete model of the probe geometry. We included the shield in our simulations as a grounded cylinder around the probe; however, this did not account for the broader PSF shape. Visual inspection of the probe reveals it is not perfectly cylindrical and has a rounded edge (see images in the [supplementary material](#)). However, simulations exploring a range of edge radii between 5 and 80 μm [illustrated by the shaded region in Fig. 2(e)] show that this alone is not enough to explain the broader PSF width and scale. High-speed video reveals subtle horizontal vibrations in addition to the vertical motion (see the [supplementary material](#)). A possible explanation for the broader PSF is that these vibrations result in a larger effective probe diameter. The difficulty in constructing an accurate model that fully reproduces the observations even in the slow-scan regime highlights the need for measuring PSFs.

05 August 2024 08:19:08

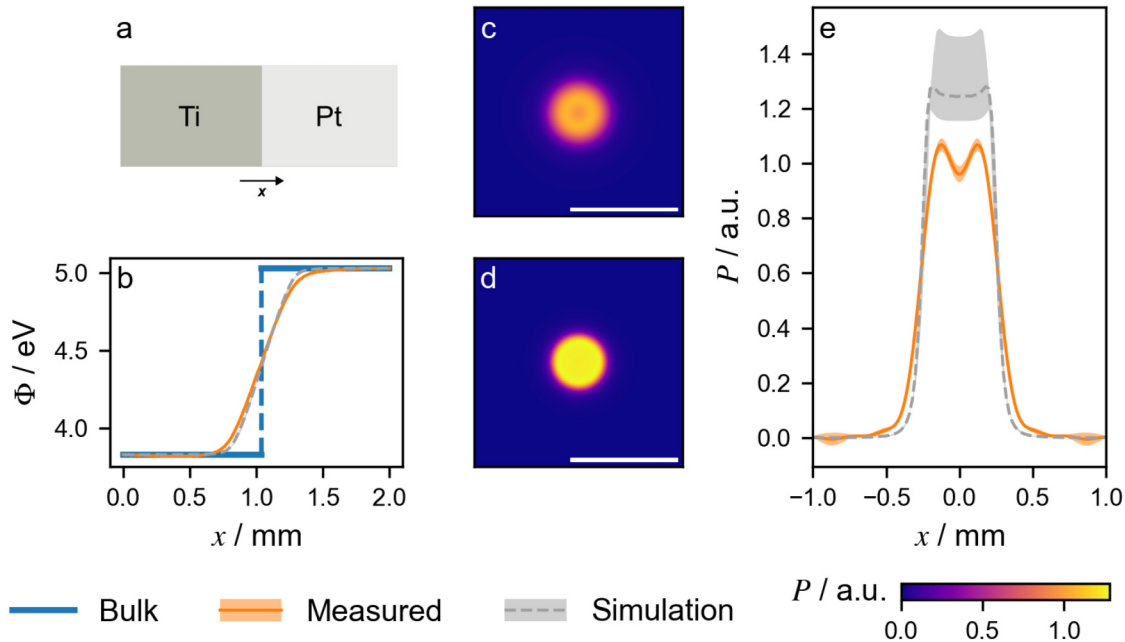


FIG. 2. Comparison between a PSF estimated using an edge measurement and a simulated PSF. (a) Scanning an edge created at the boundary between two metals with distinct work functions produces (b) an estimate for the system edge spread function (ESF) along the scan direction. (c) Shows the system PSF estimated from the ESF measurement by assuming that the probe is rotationally symmetric. (d) and (e) Simulations produce a PSF with a similar width and qualitatively similar shape but show non-negligible differences, even for a range of different probe geometries (indicated by the shaded region around the simulation line). Scale bars show 1 mm. Shaded regions on measured data represent errors estimated from standard deviation of nine scans, full details in [supplementary material](#).

With a PSF in hand, we turn our attention to reconstructing an underlying signal source from an actual measurement. [Figure 3\(a\)](#) illustrates our gold-on-silicon target, where the pattern consists a series of vertical/horizontal stripes switching between the two materials. We scan over this target at a slightly lower resolution ($80\ \mu\text{m}$ steps) and slightly larger speed ($20\ \mu\text{m}/\text{s}$ with $0.6\ \text{s}$ dwell time) so that the scan does not take unreasonably long. This produces the measured voltage map, V_m , of [Fig. 3\(b\)](#). Using [Eq. \(10\)](#) and the simulated and measured probe PSFs of [Fig. 2](#), we find that we can indeed recover estimates with improved resolution/contrast [[Figs. 3\(c\)–3\(h\)](#)]. We show in the [supplementary material](#) that these recoveries already suffer from slightly elevated scan speed; trying to eliminate temporal information in the PSF entails compromises between speed and resolution that are difficult to balance. As we show in [Sec. IV B](#), the better solution is to simply incorporate the probe motion into the PSF.

B. Determining PSFs for rapid measurements

Without compromising scan speed, we would like to be able to characterize large patterns of interest with high spatial resolution. As mentioned previously, when the distortions introduced by fast scanning are linear, then one can anticipate a velocity-dependent PSF, $P(v|x, \xi)$, that nonetheless connects the measured signal, V_m , to the underlying signal, V_s , via spatial convolution, as in [Eq. \(6\)](#). In order to acquire this PSF, we straightforwardly perform

a scan with the same measurement parameters as we use for the sample measurement. While we could repeat the procedure involving the edge PSF described above, we now no longer have to worry about scanning slowly to stay in a regime where [Eq. \(5\)](#) is applicable. Moreover, scanning fast creates an additional source of broadening to the PSF, making the use of larger targets more practical.

To get a velocity-dependent scan, we now operate the SKPM in the sweep (continuous) mode (as opposed to step mode) and with a significantly higher speed of $200\ \mu\text{m}/\text{s}$. To estimate these fast scan PSFs, we explored using 300 , 400 , and $500\ \mu\text{m}$ diameter disks. Ideally, we would want to use a target that is much smaller than the probe diameter; however, we found that the smallest disk produced a signal that was too weak. For $200\ \mu\text{m}/\text{s}$ scans, the $400\ \mu\text{m}$ disk was sufficient, but for the faster $1000\ \mu\text{m}/\text{s}$ scans, we need to use the $500\ \mu\text{m}$ diameter disk. In order to account for the finite size of the disk, we deconvolved the measured potential by a circular aperture and used a low-pass filter to remove high frequency noise. Full details are provided in the [supplementary material](#).

[Figure 4](#) shows how we put this into practice. [Figure 4\(a\)](#) shows the PSF estimated from the scan of the disk shown in the inset. As is visually apparent in the image of the PSF, the velocity dependence blurs the image in the scan direction (left to right). Next, we scan a large and detailed target ($\sim 1.5 \times 1.0\ \text{cm}^2$), as shown in [Fig. 4\(b\)](#), which again consists of gold patterned onto a silicon wafer. The scan parameters are intentionally set to be the

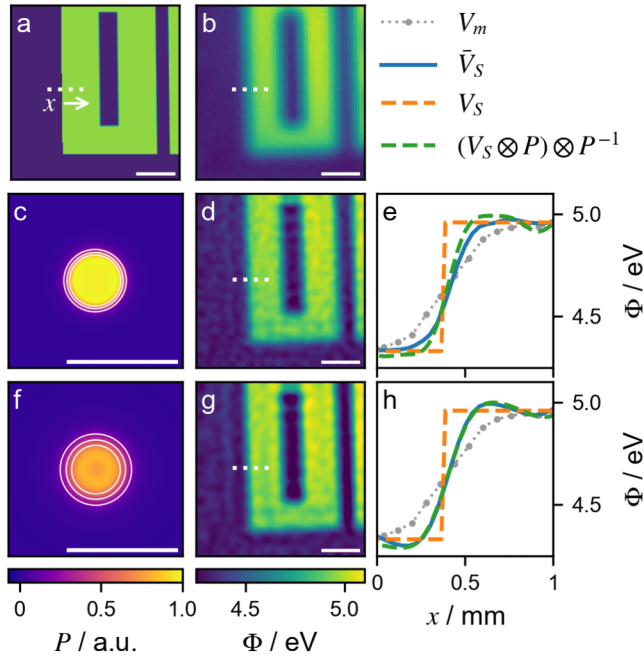


FIG. 3. Comparison between deconvolution with different PSFs in slow scans. (a) Scanning a gold-on-silicon target (V_S) with sharp features produces (b) a measured (V_m) signal with low contrast and blurred-out features. (c)–(e) Deconvolution with (c) the simulated PSF from Fig. 2(d) produces (d) an image with higher contrast; however, as shown in (e), a slice through the deconvolved image (V_S) differs from the ideal scenario ($(V_S \otimes P) \otimes P^{-1}$). (f)–(h) The experimentally measured probe PSF produces a significantly improved estimate for the original signal. Scale bars show 1 mm.

same as in the PSF of Fig. 4(a). The resulting raw voltage map is shown in Fig. 4(c). Comparing this to the slower scans of Fig. 2, the spatial blurring is much more apparent—this is, in part, due to the higher scan speed and chosen feedback parameters. Moreover, it is evident that this has the same left-to-right tail as the corresponding PSF. However, upon spatially deconvolving this scan with the corresponding PSF, the blur is reduced [Fig. 4(d)].

It is clear from these scans that the PSF shape and resulting signal depend on the acquisition speed; however, it is unclear how the observed broadening depends on the probe size, the introduction of additional noise from scanning at high speeds, the feedback system, and the scan velocity. To explore this further, Fig. 5 shows line scans of the target at different speeds using two different probes. The feedback system was tuned to give the fastest possible response to a gold–silicon work function step without introducing too much additional noise. At slow speeds, we see that these settings are sufficient to track the signal is given by a small probe scanned slowly over the same region. At high speeds, we see a significant variation in estimated work function—there is a significant lag along the scan direction. Upon deconvolving the measured signal by a PSF measured at the same speed, we see qualitatively that we recover a significantly improved estimate for the potential.

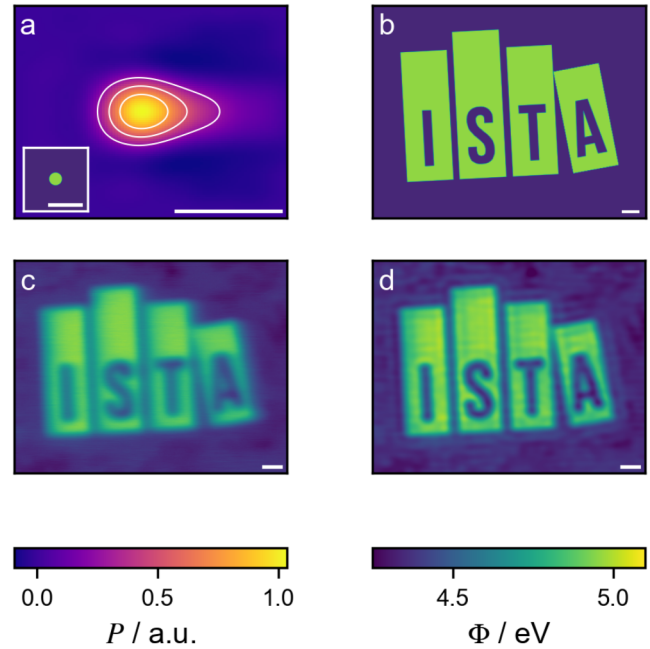


FIG. 4. PSF and deconvolution for a fast scan. (a) Fast scans produce a significantly broadened and asymmetric PSF, particularly along the scan direction. (b) and (c) When the same parameters are used to scan a large target (b), this produces a blurred-out image (c). (d) Deconvolution of the measured signal with the PSF produces a significantly improved estimate for the underlying signal. Scale bars correspond to 1 mm.

This is very apparent in a line scan across a $500\ \mu\text{m}$ diameter disk [Fig. 5(b)], where we see the slow scan produces a scan resembling the convolution of two similarly sized circular apertures, while the fast scan produces a reduced signal with a wider distribution.

Unlike in the quasi-static case, the broadening behavior here is dominated by how quickly the feedback system can respond to a change in the surface work function. Effectively, the highest resolvable spatial frequency in the scan direction is given by

$$k_x = \min \left[k_{\text{probe}}, \frac{\omega}{v} \right], \quad (12)$$

where v is the scan velocity, k_{probe} is the spatial resolution limited by the probe geometry, and ω describes the measurement cut-off frequency. The measurement cut-off frequency depends on both the response rate of the system (i.e., the SKPM oscillation frequency and PID update rate) as well as the chosen feedback parameters, which, in turn, depend on the signal-to-noise ratio. As a first order approximation, the SKPM signal scales with the probe cross-sectional area, while the noise (ignoring the effects of measurement noise) scales with the square-root of the current signal. This results in an effective bandwidth of

$$\omega \propto \Delta_V r^2, \quad (13)$$

05 August 2024 08:19:08

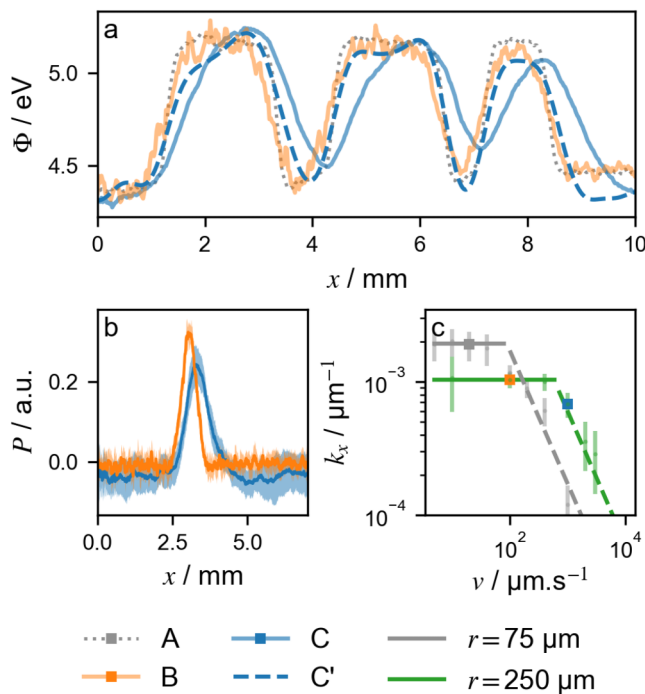


FIG. 5. Comparison between fast, deconvolved, and slow scans. (a) Partial scan across the target from Fig. 4 using (A) a $r = 75 \mu\text{m}$ radius probe scanned slowly and averaged over four scans, and single scans with a $r = 250 \mu\text{m}$ radius probe at (B) $100 \mu\text{m/s}$ and (C) $1000 \mu\text{m/s}$. (C') shows the fast scan deconvolved by a PSF estimated from scans of a $250 \mu\text{m}$ radius disk scanned using the same scan parameters. (b) Scans of the calibration disk with the large probe clearly showing the broadening due to higher scan speed. (c) The effective spatial cut-off frequency, k_x , estimated for different scan speeds (v) with two different probe radii (r) using the same scan parameters as in (a). Squares mark the scans corresponding to the speeds shown in (a) and (b). Error bars in (b) are estimated from the standard deviation of 10 scans. Error bars in (c) are estimated from the spatial frequency when the signal drops below 10% in frequency space.

where Δ_V is the minimum detectable signal. This trend is illustrated by Fig. 5(c), which shows the $1/v$ fall off at higher scan speeds and the probe size dependence in the corner frequency (additional measurements showing the noise at different velocities are included in the supplementary material). In practice, the cut-off frequency will be lower for a poorly optimized PID and other sources of noise may be dominant at different scan speeds or probe sizes.

V. CONCLUSION

In this work, we demonstrate how the PSFs relevant to scanning Kelvin probe microscopy (SKPM) can be experimentally determined. We find that measured PSFs can differ significantly from those estimated using simulations, especially for rapid scans where the finite response of the feedback system and additional noise further broaden the PSFs. We demonstrate that a practical approach for accounting for the effect of noise in a scan is to

measure the PSF using similar scan parameters to those used during measurement acquisition. We utilize two methods for estimating PSFs: one using an edge target, which provides good signal strength but only gives information about the PSF in one direction, and the second using a disk, which provides information about the full two-dimensional PSF from a single two-dimensional scan. While both methods could be used to acquire PSFs, we found that the disk was particularly useful for faster scans, where the PSFs tend to be non-axisymmetric. The edge method is more suited to acquiring lower noise PSFs but requires assumptions about the PSF symmetry or multiple measurements with different edge angles to estimate the two-dimensional PSF.

Our focus has been on characterizing the relatively large probes used in SKPM; however, the same procedure could be applicable to characterization of high speed KPFM measurements. While the larger probes used in SKPM allow direct measurement of the PSF, for smaller probes (such as those used in KPFM), the required spot size and the corresponding decrease in the signal-to-noise ratio makes experimental measurement of such PSFs difficult. We explore targets involving work function differences between metals, however, other approaches such as depositing charge spots or creating an artificial potential step²⁹ could further improve the signal-to-noise ratio. Although we focused on SKPM, this procedure could also be useful for characterizing and correcting for temporal effects in related methods.¹⁶ Additional modeling of the signal acquisition pipeline could also be useful for determining the effective measurement PSFs from simulated PSFs, this could be particularly relevant for smaller probes such as the nano-scale probes used in KPFM. The results presented here could be useful for scanning larger samples, particularly, with larger probes at faster scanning speeds while achieving decent resolution in the reconstructed images.

SUPPLEMENTARY MATERIAL

See the [supplementary material](#) for a detailed description of the experimental methods, simulations, and additional supporting figures.

ACKNOWLEDGMENTS

This project has received funding from the European Research Council (ERC) under the European Union's Horizon 2020 research and innovation program (Grant Agreement No. 949120). This research was supported by the Scientific Service Units of the Institute of Science and Technology Austria (ISTA) through resources provided by the Miba Machine Shop, Nanofabrication Facility, Scientific Computing Facility, and Lab Support Facility. The authors wish to thank Dmytro Rak and Juan Carlos Sobarzo for letting us use their equipment. The authors wish to thank the contributions of the whole Waitukaitis Group for useful discussions and feedback.

AUTHOR DECLARATIONS

Conflict of Interest

The authors have no conflicts to disclose.

Author Contributions

Isaac C. D. Lenton: Conceptualization (equal); Formal analysis (equal); Investigation (equal); Writing – original draft (equal). **Felix Pertl:** Investigation (supporting); Resources (equal). **Lubuna Shafeek:** Resources (equal). **Scott R. Waitukaitis:** Funding acquisition (equal); Supervision (equal); Writing – review & editing (equal).

DATA AVAILABILITY

The data that support the findings of this study are available from the corresponding author upon reasonable request.

REFERENCES

- ¹W. A. Zisman, “A new method of measuring contact potential differences in metals,” *Rev. Sci. Instrum.* **3**, 367–370 (1932).
- ²P. P. Craig and V. Radeka, “Stress dependence of contact potential: The ac Kelvin method,” *Rev. Sci. Instrum.* **41**, 258–264 (1970).
- ³A. Nazarov and D. Thierry, “Application of scanning Kelvin probe in the study of protective paints,” *Front. Mater.* **6**, 462587 (2019).
- ⁴A. Nazarov, M.-G. Olivier, and D. Thierry, “SKP and FT-IR microscopy study of the paint corrosion de-adhesion from the surface of galvanized steel,” *Prog. Org. Coat.* **74**, 356–364 (2012).
- ⁵H. T. Baytekin, A. Z. Patashinski, M. Branicki, B. Baytekin, S. Soh, and B. A. Grzybowski, “The mosaic of surface charge in contact electrification,” *Science* **333**, 308–312 (2011).
- ⁶X. Bai, A. Riet, S. Xu, D. J. Lacks, and H. Wang, “Experimental and simulation investigation of the nanoscale charge diffusion process on a dielectric surface: Effects of relative humidity,” *J. Phys. Chem. C* **125**, 11677–11686 (2021).
- ⁷T. Hackl, G. Schitter, and P. Mesquida, “AC Kelvin probe force microscopy enables charge mapping in water,” *ACS Nano* **16**, 17982–17990 (2022).
- ⁸Ø. G. Martinsen and A. Heiskanen, “Electrodes,” in *Bioimpedance and Bioelectricity Basics*, 4th ed., edited by Ø. G. Martinsen and A. Heiskanen (Academic Press, Oxford, 2023), Chap. 7, pp. 175–248.
- ⁹M. Nonnenmacher, M. P. O’Boyle, and H. K. Wickramasinghe, “Kelvin probe force microscopy,” *Appl. Phys. Lett.* **58**, 2921–2923 (1991).
- ¹⁰T. Glatzel, U. Gysin, and E. Meyer, “Kelvin probe force microscopy for material characterization,” *Microscopy* **71**, i165–i173 (2022).
- ¹¹W. Melitz, J. Shen, A. C. Kummel, and S. Lee, “Kelvin probe force microscopy and its application,” *Surf. Sci. Rep.* **66**, 1–27 (2011).
- ¹²A. Axt, I. M. Hermes, V. W. Bergmann, N. Tausendpfund, and S. A. L. Weber, “Know your full potential: Quantitative Kelvin probe force microscopy on nanoscale electrical devices,” *Beilstein J. Nanotechnol.* **9**, 1809–1819 (2018).
- ¹³G. Cohen, E. Halpern, S. U. Nanayakkara, J. M. Luther, C. Held, R. Bennowitz, A. Boag, and Y. Rosenwaks, “Reconstruction of surface potential from Kelvin probe force microscopy images,” *Nanotechnology* **24**, 295702 (2013).
- ¹⁴T. Machleidt, E. Sparrer, D. Kapusi, and K.-H. Franke, “Deconvolution of Kelvin probe force microscopy measurements—Methodology and application,” *Meas. Sci. Technol.* **20**, 084017 (2009).
- ¹⁵B. Ren, L. Chen, R. Chen, R. Ji, and Y. Wang, “Noise reduction of atomic force microscopy measurement data for fitting verification of chemical mechanical planarization model,” *Electronics* **12**, 2422 (2023).
- ¹⁶M. Checa, A. S. Fuhr, C. Sun, R. Vasudevan, M. Ziatdinov, I. Ivanov, S. J. Yun, K. Xiao, A. Sehirlioglu, Y. Kim, P. Sharma, K. P. Kelley, N. Domingo, S. Jesse, and L. Collins, “High-speed mapping of surface charge dynamics using sparse scanning Kelvin probe force microscopy,” *Nat. Commun.* **14**, 1–12 (2023).
- ¹⁷D. Ziegler, T. R. Meyer, R. Farnham, C. Brune, A. L. Bertozzi, and P. D. Ashby, “Improved accuracy and speed in scanning probe microscopy by image reconstruction from non-gridded position sensor data,” *Nanotechnology* **24**, 335703 (2013).
- ¹⁸R. W. Cole, T. Jimadasa, and C. M. Brown, “Measuring and interpreting point spread functions to determine confocal microscope resolution and ensure quality control,” *Nat. Protoc.* **6**, 1929–1941 (2011).
- ¹⁹S. Hudlet, M. Saint Jean, B. Roulet, J. Berger, and C. Guthmann, “Electrostatic forces between metallic tip and semiconductor surfaces,” *J. Appl. Phys.* **77**, 3308–3314 (1995).
- ²⁰F. Pertl, J. C. Sobarzo, L. Shafeek, T. Cramer, and S. Waitukaitis, “Quantifying nanoscale charge density features of contact-charged surfaces with an FEM/KPFM-hybrid approach,” *Phys. Rev. Mater.* **6**, 125605 (2022).
- ²¹C. D. Claxton and R. C. Staunton, “Measurement of the point-spread function of a noisy imaging system,” *J. Opt. Soc. Am. A* **25**, 159–170 (2008).
- ²²X. Zhang, T. Kashti, D. Kella, T. Frank, D. Shaked, R. Ulichney, M. Fischer, and J. P. Allebach, “Measuring the modulation transfer function of image capture devices: What do the numbers really mean?” *Proc. SPIE* **8293**, 64–74 (2012).
- ²³J. Ziegler and N. Nichols, “Optimum settings for automatic controllers,” *Trans. ASME* **64**, 759–768 (1942).
- ²⁴W. N. Hansen and G. J. Hansen, “Standard reference surfaces for work function measurements in air,” *Surf. Sci.* **481**, 172–184 (2001).
- ²⁵P. A. Fernández Garrillo, B. Grévin, N. Chevalier, and L. Borowik, “Calibrated work function mapping by Kelvin probe force microscopy,” *Rev. Sci. Instrum.* **89**, 043702 (2018).
- ²⁶H. N. McMurray and G. Williams, “Probe diameter and probe-specimen distance dependence in the lateral resolution of a scanning Kelvin probe,” *J. Appl. Phys.* **91**, 1673–1679 (2002).
- ²⁷U. Zerweck, C. Loppacher, T. Otto, S. Grafström, and L. M. Eng, “Accuracy and resolution limits of Kelvin probe force microscopy,” *Phys. Rev. B* **71**, 125424 (2005).
- ²⁸M. Wicinski, W. Burgstaller, and A. W. Hassel, “Lateral resolution in scanning Kelvin probe microscopy,” *Corros. Sci.* **104**, 1–8 (2016).
- ²⁹M. Brouillard, N. Bercu, U. Zschieschang, O. Simonetti, R. Mittapalli, H. Klauk, and L. Giraudet, “Experimental determination of the lateral resolution of surface electric potential measurements by Kelvin probe force microscopy using biased electrodes separated by a nanoscale gap and application to thin-film transistors,” *Nanoscale Adv.* **4**, 2018–2028 (2022).